Wavepacket dynamics for electronic quantum transport simulations

Fabiano Corsetti

Department of Physics

University of York

May 2008

Abstract

The study of quantum transport is important for understanding the propagation of electronic currents in matter on nanoscopic and mesoscopic scales. We discuss the use of a novel orthogonal wavepacket basis set for non-equilibrium many-electron transport problems. The basis is constructed from stroboscopic images of the continuous time evolution of an initial set of wavepackets. This built-in time-related feature of the basis makes it efficient for practical computational schemes and also suitable for providing physical insight into transport phenomena.

We demonstrate how the wavepacket basis can be used to recover the exact non-interacting ground state density for systems with a localised potential barrier. Using a Hartree-like electron-electron interaction, we then implement the basis in two 1D transport problems: the establishment of a steady current and the abrupt switching on of a potential barrier in a system in its ground state. Finally, we discuss the effect of spurious self-interaction on the propagation of the wavepackets.

Acknowledgements

I would like to thank: Rex Godby and Peter Bokes, for their help and guidance throughout the project; Matthieu Verstraete and Martin Stankovski, for imparting on me their *savoir-faire* in all matters physical and computational; the research group, for the time I spent working with them over the summer of 2007; Sarah Thompson, for her support; and Charlie Dyson, for several fruitful discussions.

Contents

1 Introduction **1**
- 1.1 Quantum transport and many-body simulations 1
- 1.2 Wavepacket methods 3
- 1.3 Overview 4

2 Theory **5**
- 2.1 The stroboscopic wavepacket basis set 5
  - 2.1.1 Plane wavepackets 7
  - 2.1.2 Scattered wavepackets 10
- 2.2 Applications for non-equilibrium simulations 12
  - 2.2.1 Non-interacting electrons 12
  - 2.2.2 The Hartree interaction 13

3 Methodology **15**
- 3.1 Plotting the basis functions 15
- 3.2 Calculating the propagator 16
- 3.3 Setup for non-equilibrium simulations 19

4 Results and Discussion **23**
- 4.1 Wavepacket images 23
- 4.2 Ground state density calculations 24
- 4.3 Scattering calculations 27
- 4.4 Non-equilibrium simulations 29
  - 4.4.1 Establishment of a steady current 29
  - 4.4.2 Abrupt switching on of a potential 32
  - 4.4.3 Self-interaction 33

5 Conclusions **35**
- 5.1 Accuracy and validity of results 35
- 5.2 Future work 36

List of Figures

2.1 Initial PWPs for different energy bands 8
2.2 PWP snapshots for two energy bands 9
2.3 SWP snapshots for a narrow barrier 11

3.1 Potential matrix element calculation 18
3.2 Buffer regions for many-electron simulations 21
3.3 Establishment of a steady current 21
3.4 Fortran code flowchart 22

4.1 Spurious wavepacket images 24
4.2 Convergence of the ground state density of a sodium atomic chain with a gap using SWP basis functions 25
4.3 Individual wavepacket contributions to the total density 26
4.4 Calculation of the ground state density using scattered PWP basis functions 28
4.5 Band contributions for the scattering simulation 29
4.6 Many-electron simulation of the establishment of a steady current 30
4.7 Band contributions for the establishment of a steady current . 31
4.8 Many-electron simulation of the abrupt switching on of a potential barrier 32
4.9 Electron density comparison for interacting and non-interacting electrons 33
4.10 Effect of self-interaction 34

Chapter 1

Introduction

1.1 Quantum transport and many-body simulations

Within condensed matter physics the field of quantum transport has received a growing amount of attention in recent years, becoming a very active area of theoretical and computational research. In general, it deals with the study of the behaviour of electronic currents in matter down to the level of individual electrons. This requires a rigorous theoretical framework based on the fundamental quantum mechanics of the system.

Studying the quantum nature of electronic transport is essential for understanding and predicting quantum effects such as tunnelling and the quantum Hall effect, as well as several other non-local and quantised phenomena observed in ultrasmall electronic devices over the last twenty years [1]. However, it is with the recent advent of nanotechnology and molecular electronics that quantum transport has gained particular importance; in fact, the typical sizes of electronic devices now being built are comparable to the wavefunctions of the electrons flowing through them. It is therefore necessary to use a quantum rather than classical theory of current. Applications range from single-electron transistors [2, 3] and nanowires [4] to spintronic devices [5] and research in quantum computation [6].

The quantisation of conductance in a quantum point contact (first observed experimentally in 1988 [7]) is one of a number of phenomena that can be understood by using a transport theory of non-interacting electrons, such as the Landauer-Büttiker theory [8, 9]. In this theoretical framework, the electric properties of nanoscale devices are analysed through a simplified quantum mechanical model of the system. The key idea in this case is that of semi-infinite reservoirs of electrons characterised by different electro-chemical

potentials and connected together via a narrow constriction. The system is in a state of permanent non-equilibrium, causing a current to flow through the constriction. The Landauer-Büttiker approach consists of relating the conductance to the reflection and transmission coefficients given by the scattering states of the system. A different formalism, that of Non-Equilibrium Green's Functions [8, 9], can also be used to obtain the same results.

Crucially, however, these theories neglect electron-electron interactions. When considering quantum-mechanical many-body systems these interactions are always the most problematic, making the full Hamiltonian intractable for more than a very limited number of particles. Unfortunately, many-body effects cannot generally be neglected. Therefore, in order to sufficiently reduce the computational cost of many-body simulations, several simplifying assumptions need to be introduced when developing theories of interacting electrons. These are often unjustified, and their effects on the overall simulation not well understood.

The most widely used framework for many-body simulations is given by Density Functional Theory (DFT) [10, 11]. This is an exact reformulation of the quantum mechanics of many-electron systems. Using DFT, it is possible to calculate the ground state properties of such systems by considering the electron density, rather than the much more complicated many-electron wavefunction. The system of interacting electrons is replaced by an equivalent system of non-interacting particles moving in an effective potential, which accounts for all the many-body effects. The exact form of this potential is unknown and has to be approximated. Although even very simple models of the potential are successful in many cases, this approximation presents the main difficulty in obtaining accurate and reliable results when implementing DFT.

Although the previously mentioned non-interacting theories can be used to analyse the transport properties of the fictitious system of non-interacting particles in DFT, there is no definite relationship in this case with the properties of the real system of interacting electrons. Therefore, a fully *ab initio* quantum transport theory is needed. In recent years, much work has been done on this problem by using a time-dependent formulation of DFT (TDDFT) [12]. Instead of being restricted to ground state properties, TDDFT can be used to study electron dynamics, excitations and non-equilibrium states [13, 14].

1.2 Wavepacket methods

The use of wavepacket functions is a natural choice when analysing quantum transport processes. In fact, due to their localised nature they allow for a semi-classical interpretation of the evolution of the system and the movement of the electrons involved, while at the same time providing a proper wave description of the electrons. Gaussian wavepackets, typically used in single free-electron problems, are however not ideal in the case of many-electron systems. In fact, due to the form of the wavepackets, the exclusion principle restricts the available eigenstates within each one. In other words, it is not possible to construct an orthogonal set of such wavepackets. This is important, since we are interested in populating each wavepacket with a single electron (two, including spin) in order to maintain their intuitive physical interpretation.

One of the first proposed solutions to this problem was that of using cut-off plane waves [15]. These are short pulses of finite range, and therefore normalisable. In this case it is possible to construct a set of identical pulses with non-overlapping ranges; these are necessarily orthogonal, and so can be populated to describe a uniform current flow.

A different wavepacket method, and one that has found numerous applications, is that of Wannier functions [16, 17, 18]. These are sets of localised, orthogonal functions that can be calculated by summing the Bloch states in a perfect crystal over all the values of the wavevector k within the first Brillouin zone. The resulting functions are labelled according to the band and lattice site to which they belong. One of the convenient features of this basis set is that by populating a small number of wavepackets it is possible to calculate the exact local eigenstates for a non-interacting many-electron system. However, Wannier functions have no specific advantages for time-dependent problems.

Instead, the new stroboscopic wavepacket approach discussed in this Dissertation is tailored for use in quantum transport scattering problems. This method is based on a generalisation of the wavepackets used by Martin and Landauer to analyse quantum noise in mesoscopic systems [19].The wavepacket basis is constructed in a similar way to Wannier functions; in this case, however, the complete basis set is obtained by time-evolving an initial set of appropriately chosen wavepackets through successive time steps. Therefore, for each wavepacket this will result in a collection of stroboscopic images of its time evolution. Each collection of stroboscopic images forms a separate subset of the complete basis. The images are all orthonormal, so it is possible to place a single electron in each one. Furthermore, in the subset's characteristic time step every electron in the subset will have moved

precisely from its initial image into the subsequent one. This property of the basis is particularly useful for scattering problems, since the propagation of electrons is known exactly far from the scattering potential and only needs to be calculated numerically close to it. Another advantage of the basis is that, similarly to Wannier functions, by populating a small number of wavepackets we recover the exact non-interacting many-electron ground state of the system. These properties are discussed in more detail in Chapter 2.

1.3 Overview

The aim of our investigation was to explore the properties of the stroboscopic wavepacket basis and to use the basis for 1D simulations of the propagation of electronic current through an atomic point contact. Of particular interest was the effect of including electron-electron interactions in the simulation (including spurious self-interaction), so as to assess the validity of some of the approximations used in TDDFT. Another important objective was the investigation of transient phenomena before the establishment of a steady current.

Chapter 2 will introduce the generalised theoretical description of the basis set and the special cases used for our investigations. It will then discuss how the basis can be used for non-equilibrium simulations, both for non-interacting electrons and including a simple electron-electron interaction. Chapter 3 will discuss the computational methodology for carrying out the simulations. Chapter 4 will present the results obtained and how they relate to our objectives. Finally, Chapter 5 will discuss future work needed on the simulations, including possible ways of extending the use of the basis.

A paper by P. Bokes, F. Corsetti and R. W. Godby [20] introducing the stroboscopic wavepacket basis (including its application for time-dependent quantum transport simulations discussed here) has been submitted for publication; the general definition of the basis and its formal properties follows the one in the paper.

Chapter 2

Theory

2.1 The stroboscopic wavepacket basis set

We will start with the most general definition of the wavepacket basis and then see how this can be used in practice to generate a set of localised wavepackets starting from the plane wave basis, or a set of highly non-localised (though none the less useful) split wavepackets starting from the scattering states for a square potential barrier.

We work in atomic units throughout, therefore $e = \hbar = m_e = a_0 = 1$.To define the basis set we start from a reference Hamiltonian $\hat{H}$ for an extended system with a continuous spectrum of eigenenergies ε from 0 to ∞. In general, these will correspond to a complete, orthogonal set of degenerate eigenstates $|\varepsilon, \alpha\rangle$:

$$\hat{H}|\varepsilon, \alpha\rangle = \varepsilon|\varepsilon, \alpha\rangle. \tag{2.1}$$

α may represent one or several discrete indices[1]. These eigenstates need to be normalised such that

$$\langle\varepsilon, \alpha|\varepsilon', \alpha'\rangle = \delta(\varepsilon - \varepsilon')\delta_{\alpha,\alpha'}. \tag{2.2}$$

We then generate an initial set of wavepackets by dividing the energy spectrum into a number of energy bands $\{(\varepsilon_n^\alpha, \varepsilon_{n+1}^\alpha)\}_{n=0}^\infty$ of width $\Delta\varepsilon_n^\alpha = \varepsilon_{n+1}^\alpha - \varepsilon_n^\alpha$, and integrating the original eigenstates of the reference Hamiltonian over each band as follows:

[1]In fact, for more complicated systems (such as 2D and 3D ones), α may also be a continuous index.

$$|n,0,\alpha\rangle = \frac{1}{\sqrt{\Delta\varepsilon_n^\alpha}} \int_{\varepsilon_n^\alpha}^{\varepsilon_{n+1}^\alpha} \sum_{\alpha'} U_{\alpha,\alpha'}(\varepsilon')|\varepsilon',\alpha'\rangle \, d\varepsilon'. \tag{2.3}$$

This will therefore result in a wavepacket function corresponding to each band. $U_{\alpha,\alpha'}(\varepsilon')$ is a unitary matrix that can be specified to optimise the initial set of wavepackets for a desired purpose [20]. The factor of $1/\sqrt{\Delta\varepsilon_n^\alpha}$ ensures that the wavepackets are normalised. For a given $\hat{H}$ and $U_{\alpha,\alpha'}(\varepsilon')$, the shape and spread of the wavepackets will depend on the height and width of their corresponding energy band. It should be noted that each value of α has a separate set of energy bands and wavepackets. The division of the energy spectrum into bands can be done arbitrarily, so long as the whole spectrum is covered; this allows the bands to be chosen in a convenient way depending on the system to be studied. Furthermore, the division may be different for each α (although this is usually not convenient).

Each wavepacket of this initial set is then forward and backward time-propagated:

$$|n,t,\alpha\rangle = e^{-i\hat{H}t}|n,0,\alpha\rangle. \tag{2.4}$$

Finally, by taking snapshots of this time propagation at regular intervals $\tau_n^\alpha = 2\pi/\Delta\varepsilon_n^\alpha$ for each band we generate the complete basis set

$$|n,m,\alpha\rangle = e^{-i\hat{H}m\tau_n^\alpha}|n,0,\alpha\rangle, \tag{2.5}$$

where $m = 0, \pm1, \pm2, \ldots$

The wavepacket basis is therefore composed of an infinite number of energy bands, each containing an infinite number of snapshots of the time propagation of an initial wavepacket. The basis functions can be identified by three indices: α, the energy band n in the division of the spectrum for that α, and the snapshot m within that band. The time step τ is chosen to ensure orthonormality of each snapshot within a band. Any two snapshots from different bands must also be orthogonal, since they are linear combinations of eigenstates with no eigenenergies in common (since the energy bands don't overlap).

Finally, the wavepacket basis can also be shown to be complete; in fact, any eigenstate of the reference Hamiltonian can be expanded in terms of the wavepacket snapshots of the energy band within which lies the eigenenergy of the state. This means that the wavepacket basis must be complete, since

the set of reference eigenstates is also complete. The expansion coefficients are

$$\langle n, m, \alpha | \varepsilon, \alpha \rangle = \frac{1}{\sqrt{\Delta \varepsilon_n^\alpha}} e^{i \varepsilon m \tau_n^\alpha}; \tag{2.6}$$

therefore, we obtain

$$\sum |n, m, \alpha\rangle \langle n, m, \alpha | \varepsilon, \alpha \rangle = |\varepsilon, \alpha\rangle. \tag{2.7}$$

2.1.1 Plane wavepackets

The simplest stroboscopic wavepacket basis set is derived from the conventional plane wave basis $e^{i\alpha k x}$. This basis provides a set of solutions for a flat potential (i.e. the reference Hamiltonian is simply $\hat{H} = \hat{p}^2/2$) with any energy $\varepsilon = k^2/2$. In this case $\alpha = \pm 1$, corresponding to right and left-propagating waves. To make sure these reference eigenstates satisfy (2.2), we introduce a normalising factor $1/\sqrt{2\pi k}$. Therefore,

$$|\varepsilon, \alpha\rangle = \frac{1}{\sqrt{2\pi k}} e^{i\alpha k x}. \tag{2.8}$$

Thus,

$$\langle \varepsilon, \alpha | \varepsilon', \alpha' \rangle = \frac{1}{2\pi \sqrt{k}\sqrt{k'}} \int_{-\infty}^{\infty} e^{-i(k\alpha - k'\alpha')x} \, dx. \tag{2.9}$$

Since $\alpha = \pm 1$ and $k > 0$, this becomes

$$\langle \varepsilon, \alpha | \varepsilon', \alpha' \rangle = \frac{\delta_{\alpha,\alpha'}}{2\pi \sqrt{k}\sqrt{k'}} \int_{-\infty}^{\infty} e^{-i(k - k')x} \, dx. \tag{2.10}$$

Thus,

$$\langle \varepsilon, \alpha | \varepsilon', \alpha' \rangle = \frac{\delta(k - k')\delta_{\alpha,\alpha'}}{k'}. \tag{2.11}$$

Finally, by using $\delta(k - k') = k'\delta(\varepsilon - \varepsilon')$ we obtain the desired normalisation condition stated in (2.2).

Taking $U_{\alpha,\alpha'}(\varepsilon') = \delta_{\alpha,\alpha'}$, the initial wavepacket for each energy band is given by

$$|n,0,\alpha\rangle = \frac{1}{\sqrt{2\pi\Delta\varepsilon_n^\alpha}} \int_{k_n^\alpha}^{k_{n+1}^\alpha} \sqrt{k'} e^{i\alpha k' x}\, dk'. \tag{2.12}$$

Fig. 2.1 shows some typical examples of plane wavepackets (PWP) for a range of energy bands. As can be seen from the figure, the wavepackets for narrow energy bands resemble $\mathrm{sinc}^2(x)$ functions; in fact, if we assume that the value of $\sqrt{k'}$ is approximately constant throughout the interval and equal to k_n^α, it can be shown that (2.12) becomes

$$|n,0,\alpha\rangle = \frac{1}{x}\sqrt{\frac{2k_n^\alpha}{\pi\Delta\varepsilon_n^\alpha}} \left(\cos(Ax)\sin(Bx) + \frac{i}{\alpha}\sin(Ax)\sin(Bx)\right), \tag{2.13}$$

where $A = k_n^\alpha + \Delta k_n^\alpha/2$ and $B = \Delta k_n^\alpha/2$. Taking the modulus squared we obtain

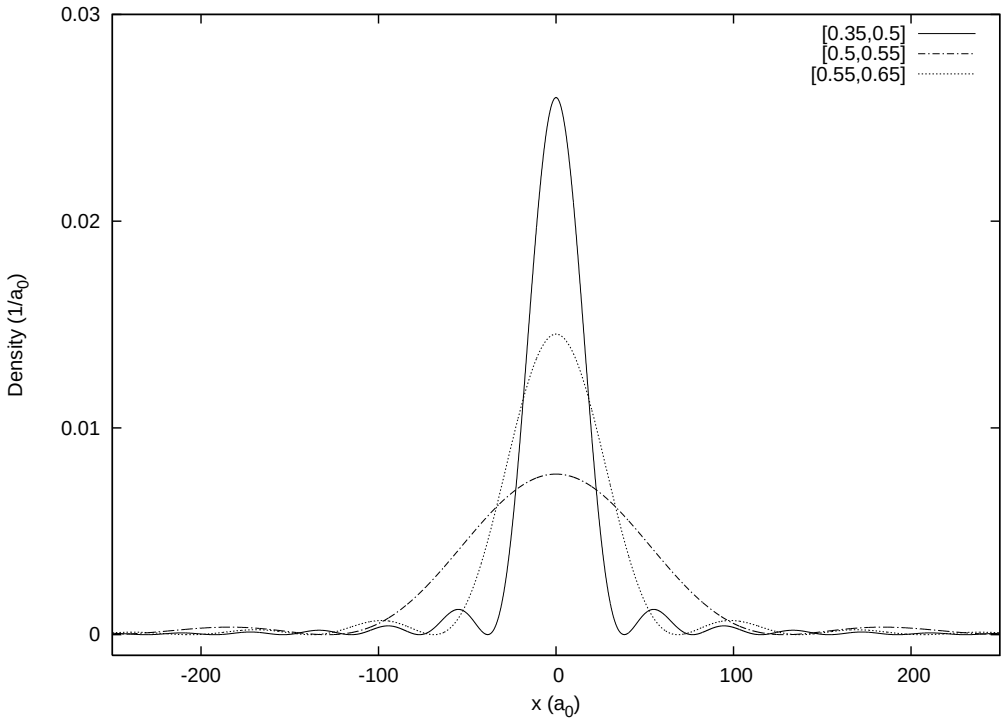

Figure 2.1: Examples of typical initial wavepackets obtained for three energy bands. The labels refer to the energy intervals used in each case (in Ha).

$$\frac{2k_n^\alpha \sin^2(\Delta k_n^\alpha x/2)}{\pi \Delta \varepsilon_n^\alpha x^2}, \tag{2.14}$$

which is a $\mathrm{sinc}^2(x)$ function as expected.

Time-propagating (2.12) for time steps τ using the time-dependent Schrödinger equation we obtain the complete set of basis functions:

$$|n, m, \alpha\rangle = \frac{1}{\sqrt{2\pi\Delta\varepsilon_n^\alpha}} \int_{k_n^\alpha}^{k_{n+1}^\alpha} \sqrt{k'} e^{i\left(\alpha k' x - \frac{k'^2}{2} m \tau_n^\alpha\right)} \, dk'. \tag{2.15}$$

Fig. 2.2 shows two sets of snapshots for different energy bands.

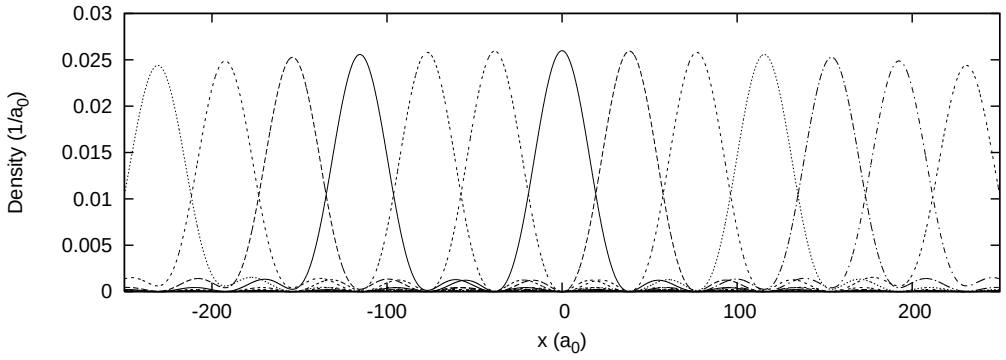

(a) $[0.35, 0.5]$

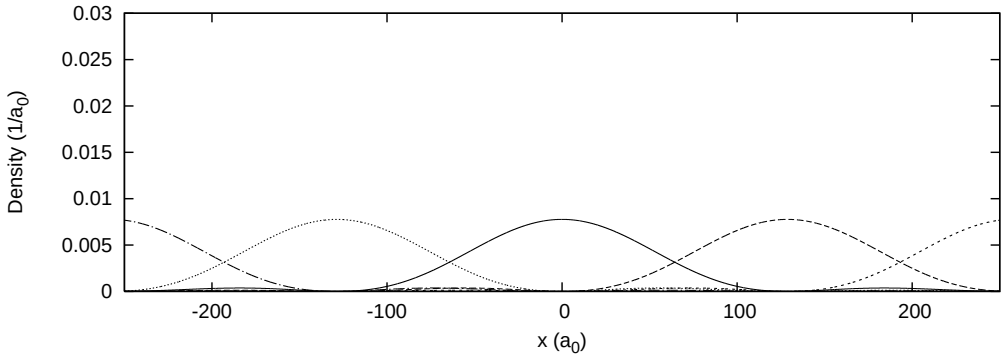

(b) $[0.5, 0.55]$

Figure 2.2: Sets of snapshots (i.e. stroboscopic images) of the time evolution of the initial wavepacket for two energy bands; these are used to construct the subsets of the complete basis. For band (a) a slight dispersion of the wavepackets is noticeable.

We can now easily show that these functions are orthonormal with respect to m:

$$\langle n, m, \alpha | n, m', \alpha \rangle = \frac{1}{\Delta\varepsilon_n^\alpha} \int_{k_n^\alpha}^{k_{n+1}^\alpha} k' e^{i\frac{k'^2}{2}\tau_n^\alpha (m-m')}\, dk'. \tag{2.16}$$

Changing the integration variable, this becomes

$$\begin{aligned} \langle n, m, \alpha | n, m', \alpha \rangle &= \frac{1}{\Delta\varepsilon_n^\alpha} \int_{\varepsilon_n^\alpha}^{\varepsilon_{n+1}^\alpha} e^{i\varepsilon'\tau_n^\alpha (m-m')}\, d\varepsilon' \\ &= \delta_{m,m'}. \end{aligned} \tag{2.17}$$

2.1.2 Scattered wavepackets

The plane wavepackets are constructed from the eigenstates of a flat reference potential; similarly, we can choose to use the scattering states for a potential step or barrier. We consider the case of a square barrier. The reference potential is now

$$V(x) = \begin{cases} V_0, & |x| \le a \\ 0, & |x| > a; \end{cases} \tag{2.18}$$

the scattering states can be thought of as electron "beams" being partially transmitted through the barrier and partially reflected off it. The incident, transmitted and reflected beams are all represented by plane waves $e^{\pm ikx}$ with appropriate sign. Therefore, on the incident side the wavefunction is

$$\psi(x) = Ae^{ikx} + Be^{-ikx}. \tag{2.19}$$

Inside the barrier the wavefunction has a similar form:

$$\psi(x) = Ce^{i\kappa x} + De^{-i\kappa x}, \tag{2.20}$$

where $\kappa = \sqrt{2(\varepsilon - V_0)}$. On the transmitted side the wavefunction is

$$\psi(x) = Ee^{ikx}. \tag{2.21}$$

By equating the wavefunction and its derivative at the sides of the barrier we can solve for the coefficients B, C, D, E in terms of A, k, V_0, a. The scattering

states can now be integrated for each energy range and time-propagated as before to obtain the complete basis set of scattered wavepackets (SWP)

$$|n, m, \alpha\rangle = \frac{1}{\sqrt{2\pi\Delta\varepsilon_n^\alpha}} \int_{k_n^\alpha}^{k_{n+1}^\alpha} \sqrt{k'} \left(C_1(k') e^{ik''x} + C_2(k') e^{-ik''x} \right) e^{-i\frac{k'^2}{2} m \tau_n^\alpha} \, dk', \tag{2.22}$$

where $k'' = \kappa$ inside the barrier and k elsewhere.

Fig. 2.3 shows SWP snapshots for a typical energy band. For $m < 0$, i.e. for backward time propagation, a single wavepacket approaches the barrier on the incident side. Far away from the barrier the SWP is approximately equal to its PWP counterpart; however, as it approaches the barrier (and m is still negative but small, close to the initial wavefunction $m = 0$), the wavepacket becomes distorted. Once it has passed the barrier ($m > 0$), the SWP splits into two components, one moving forward (the transmitted part) and one backward (the reflected part). Once again as the two components have moved far away from the barrier they become PWPs again, with amplitudes equal to the reflection and trasmission probabilities $R = |B/A|^2$ and $T = |E/A|^2$. Therefore, the SWPs become delocalised for $m > 0$, although instead of being spread throughout the whole system they are simply split into two localised components.

Similarly to the PWP basis, which has right and left-going PWPs, the SWP basis has right and left-incident SWPs for each energy band. The direction of propagation is determined by α.

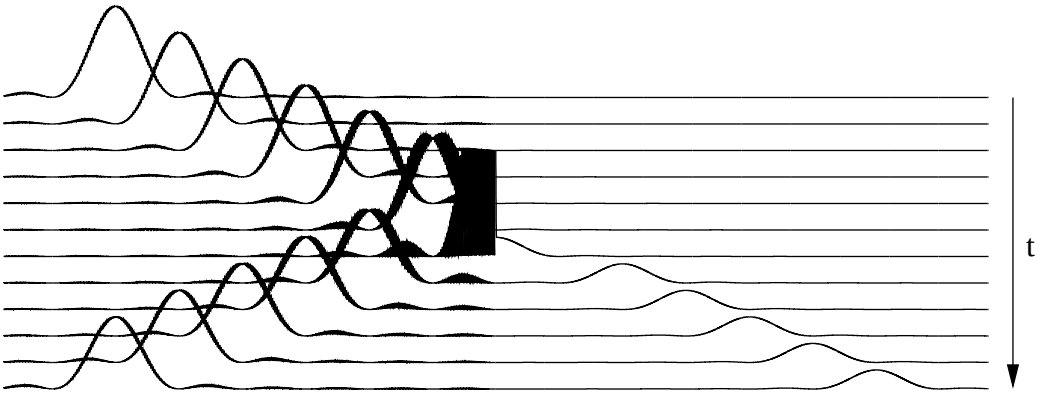

Figure 2.3: Snapshots of the time evolution of a SWP (using energy band $[0.5, 0.55]$) due to a narrow barrier. $V_0 = 0.75$Ha and $a = a_0$. There is a noticeable phase shift in the transmitted component of the wavepacket.

2.2 Applications for non-equilibrium simulations

2.2.1 Non-interacting electrons

We have seen that an electron can be placed in a single wavepacket, and that in a time-independent potential equal to the reference potential for the basis it will propagate exactly from one wavepacket to the next in time τ. In the simplest case, for a flat potential we obtain PWPs which are highly localised, regularly spaced throughout the system and propagate with little dispersion over a short range. These can be used in numerical simulations to study the time-dependent dynamics of electrons scattering through an arbitrary localised potential. In fact, far away from the potential obstacle the electrons are in an extended region of flat potential, and so the PWPs are approximate eigenstates of the system (as seen in the SWP basis). In this region the exact time evolution of the current is known and does not need to be simulated; it is only necessary to perform a numerical propagation once the electron is in the central region of localised potential. However, after being scattered through this obstacle the wavepacket will leave the central region and return to the flat regions on either side, therefore also returning to the exact PWP propagation.

The propagation of electrons in a potential can be simulated by using a quantum mechanical evolution operator known as a propagator. The propagator time-evolves the system as follows:

$$\varphi(t) = \hat{U}(t, t_0)\,\varphi(t_0)\,. \tag{2.23}$$

By substituting this into the time-dependent Schrödinger equation, we see that for a time-independent Hamiltonian the propagator simply becomes

$$\hat{U}(t + \Delta t, t) = e^{-i\Delta t\hat{H}}. \tag{2.24}$$

This unfortunately restricts us to the case of non-interacting electrons, as electron-electron interactions will add time-dependent terms to the Hamiltonian. It should be noted that the exponential of a matrix $\hat{A}$ is defined in terms of the Taylor expansion

$$e^{\hat{A}} = \sum_{n=0}^{\infty} \frac{\hat{A}^n}{n!}; \tag{2.25}$$

in practice, this will need to be approximated.

One of the main desirable properties of the wavepacket basis is that is it possible to recover the exact non-interacting many-electron ground state density of a system whose Hamiltonian is equal to the reference Hamiltonian for the basis set simply by occupying all the basis functions (i.e. summing the contributions of all the stroboscopic images) in the energy bands below the Fermi energy E_{F}. Furthermore, since the wavepackets are highly localised it is only necessary to consider for each band a small number of them lying within a region of interest; in this way it is possible to calculate a good approximation of the local ground state density by using very few basis functions.

In the case of a localised potential not equal to the reference one it is also possible to calculate the ground state density in a similar fashion, since we know that far away from the central region of non-flat potential the density will be approximately flat (i.e. equal to the ground state density for a flat potential). Therefore, we can populate the edges of the system with PWPs up to E_{F} and then let them propagate through the central region (both for right and left-incident wavepackets); once a steady current spanning the whole central region has been established in both directions the system will be in its ground state. This must be the case since the edges of the system are fixed to the correct flat ground state.

2.2.2 The Hartree interaction

The numerical propagation method for non-interacting electrons can be extended to include the effects of electron-electron interactions. The first step towards a full *ab initio* simulation (using for example TDDFT) is the addition of a time-dependent Hartree term to the static potential. The Hartree potential is of the form

$$V_i^{\mathrm{H}}(\mathbf{r}) = \sum_{j \neq i}^{N} \int \frac{|\psi_j(\mathbf{r}')|^2}{|\mathbf{r} - \mathbf{r}'|} \, d^3\mathbf{r}'; \tag{2.26}$$

each electron, therefore, feels a Coulomb repulsion from the average position of all the others. Replacing the sum with the electron density $n(\mathbf{r})$, we obtain

$$V_i^{\mathrm{H}}(\mathbf{r}) = \int \frac{n(\mathbf{r}')}{|\mathbf{r} - \mathbf{r}'|} \, d^3\mathbf{r}'. \tag{2.27}$$

However, this introduces a self-interaction problem, since n will also include the contribution to the density from the electron feeling the potential. To

eliminate this problem we would need to subtract the contribution of each electron in turn from the total density; in practice, however, this is generally ignored due to the added computational cost.

A further problem is that the Hartree potential is not well-defined in 1D. In fact, at $x = x'$ the integrand is undefined, causing singularities to appear in the potential. Instead, in 2D and 3D systems the singularities are removed by the integration.

Therefore, instead of the Hartree potential we shall use a similar point interaction term:

$$\begin{aligned} V_i^{\mathrm{H}}(x) &= W \int_{-\infty}^{\infty} n(x')\delta(x - x')\, dx' \\ &= W n(x), \end{aligned} \tag{2.28}$$

where W is an arbitrary weighting. This term is well-defined since it is simply proportional to the electron density. Although it is not an accurate representation of the Coulomb interaction it does preserve the main idea of the Hartree potential, namely, that electrons will tend to be repelled from regions of higher density to regions of lower density.

After the addition of the Hartree term to the potential, the Hamiltonian for the system becomes time-dependent; therefore, the definition of the propagator from (2.24) is no longer exact. However, if we consider sufficiently small time intervals Δt over which $\hat{H}$ is approximately constant this definition can still be used for the numerical propagation scheme. However, in this case it will be necessary to update $\hat{H}$ after each time step (since the electron density and therefore the potential will have changed).

Chapter 3

Methodology

3.1 Plotting the basis functions

As shown in Chapter 2, both the PWPs and SWPs are obtained by integrating plane waves (or combinations of plane waves) over a small k range with appropriate weightings. In both cases the integral is non-analytic; therefore, it is necessary to perform a numerical integration. There are several different families of algorithms to do so; for the purpose of plotting the wavepackets, an extended closed Newton-Cotes method was chosen.

The Newton-Cotes family of methods for numerical integration is based on the evaluation of the integrand at equally spaced points. The two simplest methods in this family, known as the trapezium rule and Simpson's rule, fit a linear or quadratic polynomial to the evaluated points. These are closed methods, since the integrand is evaluated at the endpoints of the interval. Extended methods subdivide the interval and apply one of the basic methods repeatedly to each subinterval.

The specific extended formula used for integrating over the k bands is

$$\begin{aligned}\int_{k_1}^{k_N} f(k)\,dk = \delta k \Bigg[&\frac{3}{8}k_1 + \frac{7}{6}k_2 + \frac{23}{24}k_3 + \sum_{i=4}^{N-3} k_i \\ &+\frac{23}{24}k_{N-2} + \frac{7}{6}k_{N-1} + \frac{3}{8}k_N\Bigg] + O\left(\frac{1}{N^4}\right).\end{aligned} \tag{3.1}$$

This formula can be derived by fitting cubic polynomials through successive overlapping groups of four points [21]. The error estimate for this method is equal to that of an extended Simpson's rule; however, (3.1) has the computational advantage that only the first and last three points need to be

multiplied by a coefficient, while the great majority of the points simply need to be summed. This is not the case for Simpson's rule.

Since we are integrating plane waves over a range of k, we know that the integrand will be an oscillating function with $\lambda = 2\pi/x$. Therefore, depending on the x range being plotted it is possible to calculate the smallest wavelength of the integrand and hence choose the value of the sampling step δk accordingly (so as to be $< \lambda$).

While plotting the PWPs is a straightforward application of (3.1) to (2.15), the SWPs present a number of extra complications. In fact, the integrand in (2.22) is now a sum of both right and left-going plane waves with coefficients C_1 and C_2, which depend on k and x (i.e. equal to A and B on the incident side of the barrier, C and D inside the barrier, and E and zero on the transmitted side). Therefore, the coefficients have to be calculated for each k value needed for the numerical integration, and the correct two have to be selected each time x enters a new region. Furthermore, the wavevector is also dependent on x, since inside the barrier it is modified by V_0. To make the whole process more efficient, the values of the coefficients for the entire k range are stored in an array and reused when plotting each new x point.

3.2 Calculating the propagator

The propagator matrix is needed for any non-equilibrium simulation. During the simulation, the state vector for each electron is time-evolved by a small time step Δt when premultiplied by the propagator. The form of the propagator is given by (2.24). As already noted, the exponential of the Hamiltonian is defined by a Taylor expansion. For the purpose of the numerical simulation, we can neglect terms smaller than $\hat{H}^4$. This is conditionally stable [22] and relatively fast to calculate even for large matrices. Therefore, to obtain the propagator we need to first calculate the Hamiltonian for the system. It is convenient to consider the kinetic and potential terms separately:

$$\hat{H} = \hat{T} + \hat{V} \tag{3.2}$$

Therefore, the kinetic matrix elements are given by

$$T_{mn} = \frac{1}{2}\int_{-\infty}^{\infty} \psi_m^* \frac{\partial^2}{\partial x^2}\psi_n \, dx, \tag{3.3}$$

and the potential matrix elements by

$$V_{mn} = \int_{-\infty}^{\infty} \psi_m^* V(x) \psi_n \, dx. \tag{3.4}$$

Firstly we consider the kinetic matrix. We can show that the matrix element for any two basis functions within the same energy band (and with the same α) only depends on the difference between their snapshot numbers $m-m'$. In fact, considering the time derivative of the matrix element between two functions, we find that

$$\begin{aligned}
\frac{\partial}{\partial t} \int \psi_m^* \hat{H} \psi_n &= \int \left\{ \left[\frac{\partial}{\partial t} \psi_m \right]^* \hat{H} \psi^n + \psi_m^* \hat{H} \left[\frac{\partial}{\partial t} \psi_n \right] \right\} d^3\mathbf{r} \\
&= \int \left\{ \left[\frac{1}{i} \hat{H} \psi_m \right]^* \hat{H} \psi_n + \psi_m^* \hat{H} \left[\frac{1}{i} \hat{H} \psi_n \right] \right\} d^3\mathbf{r} \\
&= \frac{1}{i} \int \left\{ -\psi_m^* \hat{H}^2 \psi_n + \psi_m^* \hat{H}^2 \psi_n \right\} d^3\mathbf{r} \\
&= 0.
\end{aligned} \tag{3.5}$$

For $V = 0$, $\hat{H} = \hat{K}$ and so any basis function m time-evolves into $m + 1$ in time step τ; therefore, for two basis functions, $m - m'$ at each time step stays constant. Since we have shown that their matrix element also has to stay constant, it follows that any two basis functions with the same $m - m'$ must have the same matrix element. Furthermore, since the kinetic matrix does not depend on V, this must also apply to cases in which $V \neq 0$. Therefore, the kinetic matrix simplifies to

$$\hat{T} = \begin{bmatrix}
T_{00} & T_{01} & T_{02} & \cdots & T_{0N} \\
T_{01}^* & T_{00} & T_{01} & \cdots & T_{0(N-1)} \\
T_{02}^* & T_{01}^* & T_{00} & \cdots & T_{0(N-2)} \\
\vdots & \vdots & \vdots & \ddots & \vdots \\
T_{0N}^* & T_{0(N-1)}^* & T_{0(N-2)}^* & \cdots & T_{00}
\end{bmatrix}. \tag{3.6}$$

Using the PWP basis, the value of the matrix elements can be calculated analytically:

$$
\begin{aligned}
K_{0n} &= \frac{1}{4\pi\Delta\varepsilon}\int_{k}^{k+\Delta k}\int_{k}^{k+\Delta k} k'^{\frac{1}{2}}k''^{\frac{5}{2}}e^{-i\frac{k''^2}{2}n\tau}\left[\int_{-\infty}^{\infty}e^{-i(k'-k'')x}\,dx\right]dk'\,dk'' \\
&= \frac{1}{2\Delta\varepsilon}\int_{k}^{k+\Delta k}\int_{k}^{k+\Delta k} k'^{\frac{1}{2}}k''^{\frac{5}{2}}e^{-i\frac{k''^2}{2}n\tau}\delta\left(k'-k''\right)\,dk'\,dk'' \\
&= \frac{1}{2\Delta\varepsilon}\int_{k}^{k+\Delta k} k'^{3}e^{-i\frac{k'^2}{2}n\tau}\,dk' \\
&= \frac{1}{\Delta\varepsilon}\int_{\varepsilon}^{\varepsilon+\Delta\varepsilon}\varepsilon' e^{-i\varepsilon' n\tau}\,d\varepsilon'.
\end{aligned}
\tag{3.7}
$$

This derivation also shows that any matrix element between basis functions in separate energy bands must be zero. In fact, since the two integrals would be over different intervals, the delta function would always be zero.

Unfortunately, the potential matrix elements can't be derived analytically using the same approach; therefore, a numerical integration is employed, using the same algorithm as for the basis function calculations. In this case, the use of localised wavepackets is very useful, since it is possible to significantly reduce the computational cost by employing a cut-off range from the central peak. By doing so only two small regions of space need to be considered for the integration, as shown in Fig. 3.1.

Calculating the matrix elements using the SWP basis is very similar to the method used for PWPs. In this case, however, the SWPs don't time-evolve into each other in a zero potential. Instead, they do so in a system in which the potential is equal to the reference potential used to construct

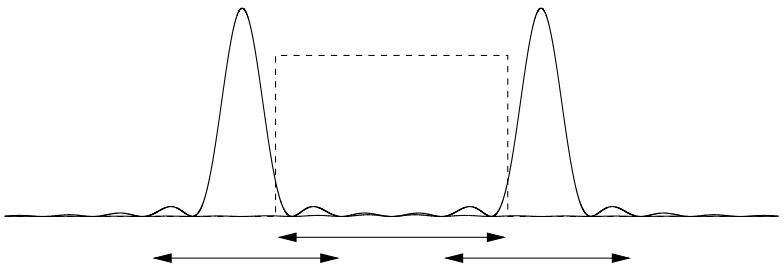

Figure 3.1: Potential matrix element calculation between two localised wavepackets for a square barrier potential. By employing a cut-off distance from the peak of the wavepackets it is only necessary to integrate over the two small overlapping sections of the three ranges.

the basis set. For this setup, the proof that the matrix elements only depend on $m - m'$ is still valid; furthermore, we can show that they are equal to the corresponding kinetic matrix elements for PWPs. This is because a long time before hitting the barrier ($m \ll 0$), the SWPs tend to PWPs, and so must have the same matrix elements. However, using the argument that the elements only depend on $m - m'$, we see that there can't be any difference between the SWP elements far away from the barrier and close to it. Therefore, for this setup the SWP total matrix and the PWP kinetic matrix are completely identical.

This result can still be used when the system potential is not equal to the reference potential. The Hamiltonian can now be rewritten as

$$\begin{aligned} \hat{H} &= \left(\hat{K} + \hat{V}_0\right) + \left(\hat{V} - \hat{V}_0\right) \\ &= \hat{K}^{\mathrm{PWP}} + \Delta\hat{V}, \end{aligned} \tag{3.8}$$

where V_0 is the reference potential and ΔV_{mn} is the matrix element obtained by using the difference between the two potentials $\Delta V = V - V_0$.

Finally, for the case of a time-dependent propagator (with the addition of the Hartree term to the potential), we need to recalculate the potential matrix after each time step, although the kinetic matrix is unchanged. In practice, provided that the electron density of the system changes sufficiently slowly, we only need to update the propagator at regular intervals $N\Delta t$. The time-dependent potential matrix elements are given by

$$V_{mn} = \int_{-\infty}^{\infty} \psi_m^* \left(\Delta V + V^{\mathrm{H}}\right) \psi_n \, dx, \tag{3.9}$$

where V^{H} is calculated from (2.28).

3.3 Setup for non-equilibrium simulations

We have shown how to calculate the wavepacket basis functions and the propagator matrix for the purpose of a simulation. Two principle setups were investigated: the abrupt switching on of a potential barrier in a system in equilibrium, and the establishment of a steady current in a system starting in its ground state by injecting a file of right-going electrons in an unoccupied energy band.

Although the propagator matrix is stable and sufficiently accurate for our purposes[1], the finite nature of the simulations introduces a problematic and unphysical effect in its behaviour. In fact, once an electron propagated through the system reaches one of the edges, it "bounces back" to the other edge. This is an inevitable consequence of the requirement on the propagator to be unitary. In fact, considering our numerical propagation as part of an extended system, we know that once an electron reaches the edge of the simulated range it should pass into the analytic region and continue propagating forwards exactly from one basis function to the next. However, since this analytic region is not included in the simulation, we simply require it to disappear after reaching the last wavepacket that is being used. Instead, to preserve its normalisation it bounces back to the first wavepacket at the other end of the system and continues moving as before. Furthermore, due to the nature of the propagation from one basis function to the next, the electron wavepacket becomes distorted when approaching the edge.

This issue is resolved by manually removing electrons approaching the edges of the system. Since each electron stays localised and the time taken for it to propagate through the system is known, this can be done easily and with little disruption to the total density close to the central barrier. Therefore, each electron is propagated for a limited time, after which it is assumed that it has passed into the analytic regions outside the range of the simulation and so is removed. This assumption is generally valid for narrow, simple barriers (ones not supporting bound states), since only a small phase shift will be introduced in the transmitted and reflected wavepackets.

Buffer regions also need to be introduced at either side of the system. These are assumed to be in the analytic region and so don't need to be populated with electrons; their purpose is simply to allow the electrons inside the actual system to propagate up to the last basis function without distortion, and to further prevent the possibility of any components reaching the edges and bouncing back. Therefore, the electron density should always be close to zero in the buffer regions. However, since they are actually part of the analytic region, when calculating the Hartree potential the density needs to be fixed to the exact flat ground state density for the system (Fig. 3.2).

By implementing buffer regions and propagating electrons for a finite time before removing them, it is possible to use the wavepacket basis set effectively to investigate time-dependent quantum transport phenomena. The simplest case to be considered is that of a system in it ground state being perturbed

[1]It is possible to converge the propagator matrix elements to their true values i.e. for the case in which all the basis functions are included in the energy bands present. The difference was found to be negligible compared with other sources of error (such as the accuracy of the basis functions and finite system size effects).

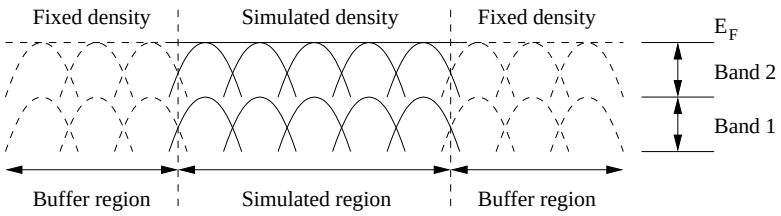

Figure 3.2: Use of buffer regions in many-electron simulations. Although the wavepackets are unoccupied in these regions, the electron density used to calculate the Hartree potential is fixed to the correct value for full bands.

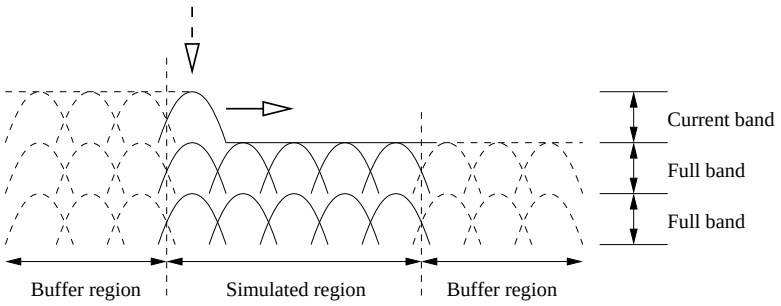

Figure 3.3: Setup for simulating the establishment of a steady current in an empty energy band. Right-propagating electrons are injected into the system every τ in the left-most wavepacket within the simulated region.

by the introduction of a potential barrier. Initially, $V = 0$; therefore, it is sufficient to use a PWP basis and start the simulation by populating each wavepacket in the system up to E_{F} with an electron. With the introduction of the barrier at $t = 0$ both right and left-going electrons will start being scattered, producing oscillations in the electron density. After a sufficiently long time we expect these transient effects to settle into a new steady state, equal to the ground state obtained by populating SWPs constructed from the same potential barrier. This method can also be used starting from a system with a steady current (i.e. with an energy band full for right-going wavepackets and empty for left-going ones).

Another simulation to be considered is the establishment of a steady current (Fig. 3.3). In this case, the system starts in its ground state as before; however, instead of introducing a perturbing barrier, right-going electrons are manually added in an empty energy band from the left side of the system every time step τ. This creates a file of electrons propagating through the central region; once they span the entire range of the system (and so

start being removed from the right side), we expect a steady current to be established.

Fig. 3.4 shows a flowchart of the main structure of the Fortran code written to implement the wavepacket basis in non-equilibrium simulations; it includes all the methods discussed in this chapter.

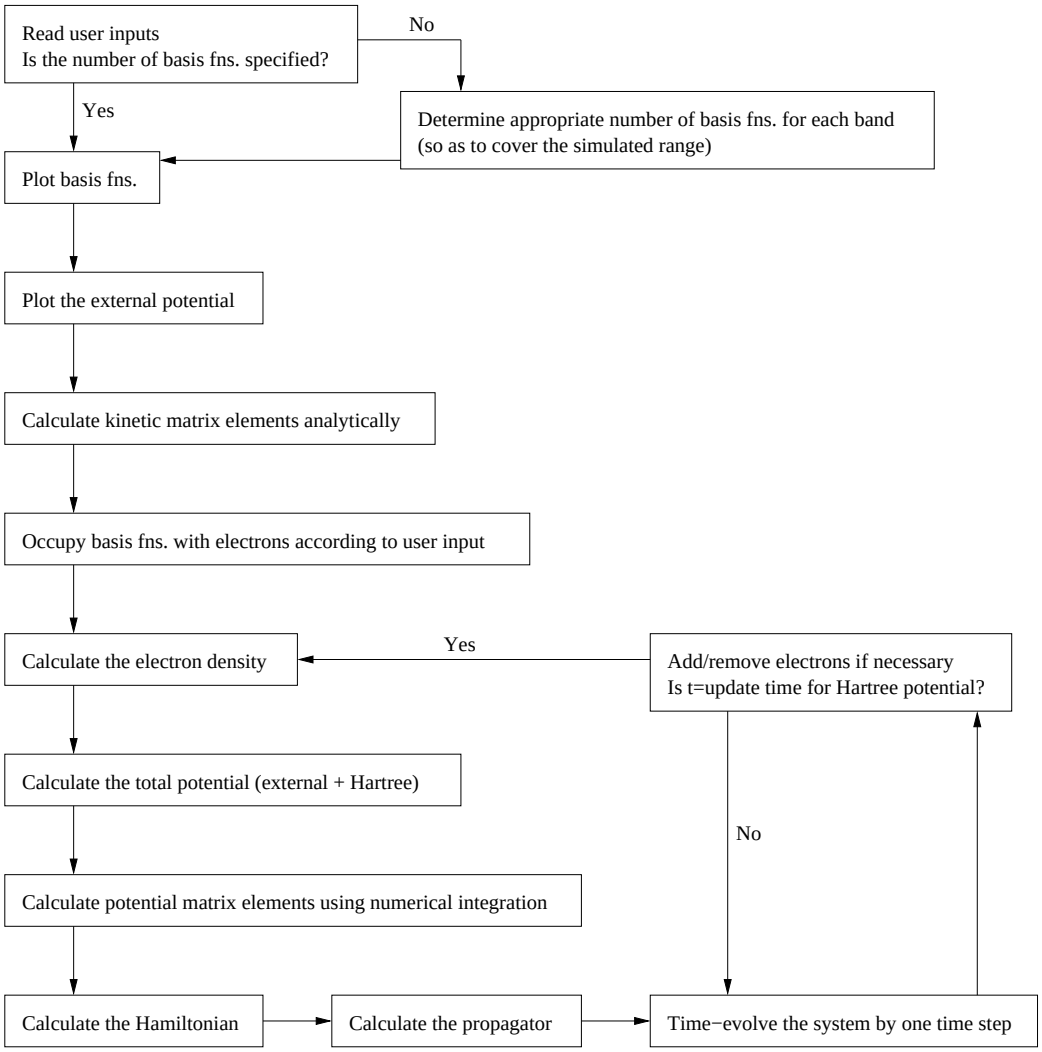

Figure 3.4: Flowchart representation of a time-dependent simulation.

Chapter 4

Results and Discussion

4.1 Wavepacket images

A few typical wavepacket plots, obtained by using the numerical integration method discussed previously, have already been shown in Chapter 2 (Figs. 2.1, 2.2 and 2.3). Before proceeding to the results of calculations using the wavepackets, it is worth briefly discussing a potential pitfall of this numerical method.

It was noted when plotting the basis functions over large x ranges that exact images of the original wavepacket appear on either side of it, at equally spaced intervals L. Furthermore, the distance between images increases with decreasing δk (the sampling step used in the numerical integration), as shown in Fig. 4.1.

This anomaly can be understood by considering the effect of approximating an integral with a sum. The original definition of the PWPs is similar to a continuous Fourier transform; this results in an aperiodic function[1]. On the other hand, the numerical integration changes this definition to a discrete Fourier transform, which is necessarily periodic. The period can be shown to be $2\pi/\delta k$; this is equal to the observed image distance. Therefore, when using the wavepacket basis it is always necessary to ensure that δk is small enough to prevent spurious images from affecting the simulation; fortunately, since L is known, this is easily done.

[1]In fact, if we assume $\sqrt{k'}$ is constant throughout the interval, we obtain the Fourier transform of a box function, which is a $\mathrm{sinc}(x)$ wavepacket as expected.

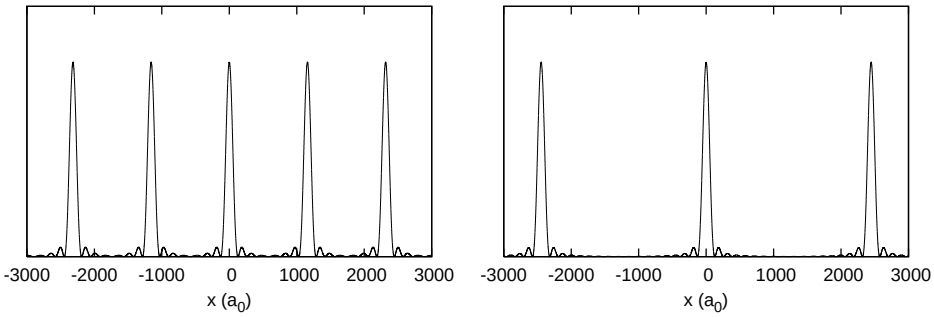

(a) $\delta k = 0.005 a_0^{-1}$ (b) $\delta k = 0.0025 a_0^{-1}$

Figure 4.1: Single basis function plotted over a large x range. As the accuracy of integration is increased, the images move further away from the real wavepacket (at $x = 0$). The distance between images is $L = 2\pi/\delta k$.

4.2 Ground state density calculations

One of the useful features of using the wavepacket basis is the possibility of recovering the exact local non-interacting many-electron ground state density simply by summing contributions from a small number of wavepackets. In the case of a system characterised by a Hamiltonian equal to the reference Hamiltonian for the basis it is enough to occupy with an electron each wavepacket localised within the region of interest. Due to their localised nature, the contributions from all other wavepackets can be neglected.

As an example, we consider the ground state density of a 1D jellium model of a chain of sodium atoms with a gap. The potential for this system is a square barrier, such as (2.18). It is therefore possible to construct a set of SWPs using the same potential. The distance between sodium atoms in the chain is $a = 4.68 a_0$. The Fermi energy is $E_{\mathrm{F}} = 0.056$Ha and the potential height is $V_0 = 0.05$Ha. The jellium model ground state density can be calculated exactly using a Green's function method [20].

Using the SWP basis, any energy bands higher than E_{F} are going to be completely empty and so need not be considered at all. For energies lower than E_{F}, we have chosen to divide the energy spectrum into two bands: the lower band, covering the interval $(0, 0.025]$, and the higher band, covering $[0.025, 0.056]$. Each band has right and left-incident wavepackets.

Fig. 4.2 shows how the SWP density converges to the exact density as the number of basis functions included in the calculation increases. Within each band, the wavepackets are denoted by the snapshot number m. $m = 0$ is the band's initial wavepacket (equivalent to $t = 0$); $m < 0$ denotes backwards time propagation and $m > 0$ forwards time propagation. In Fig. 4.2, N

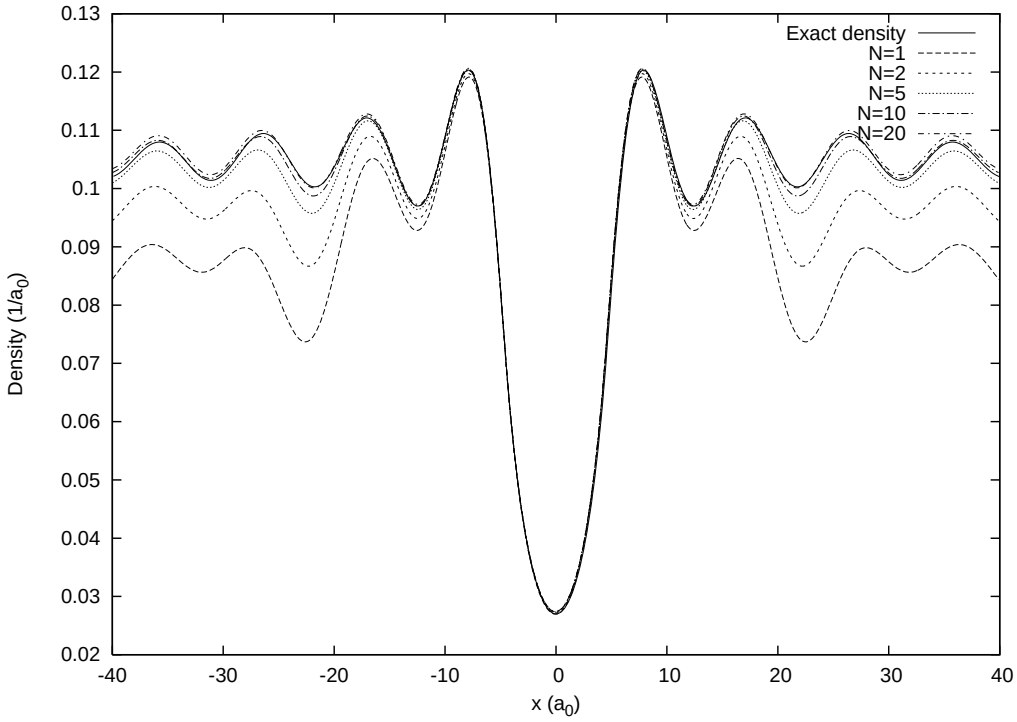

Figure 4.2: Convergence of the ground state density of a sodium atomic chain with a gap using SWP basis functions.

denotes the number of snapshots used on either side of the intial wavepacket (for example, the $N = 2$ calculation sums contributions for $m = 0, \pm 1, \pm 2$ for each band). Therefore, the total number of wavepackets plotted for each calculation is $2(2N + 1)$. Right and left-incident wavepackets are simply reflected about $x = 0$ (due to the symmetry of the potential) and so don't need to be plotted separately.

As can be seen from the figure, the density within a few Fermi wavelengths rapidly converges as N increases ($\lambda_{\mathrm{F}} = 18.8a_0$). A good agreement is obtained for $N > 10$ (i.e. using at least 22 wavepackets). It should be noted that the density calculated for $N = 20$, although close to the exact density, is in fact slightly too high; this obviously cannot be corrected by adding more wavepackets. Instead, the discrepancy is due to the numerical integration, the accuracy of which needs to be increased to further converge the results.

Fig. 4.3 shows how the various wavepackets in the two energy bands contribute to the total density. Only the right-incident wavepackets are shown; their contribution is small on the transmitted side of the barrier. Instead, on

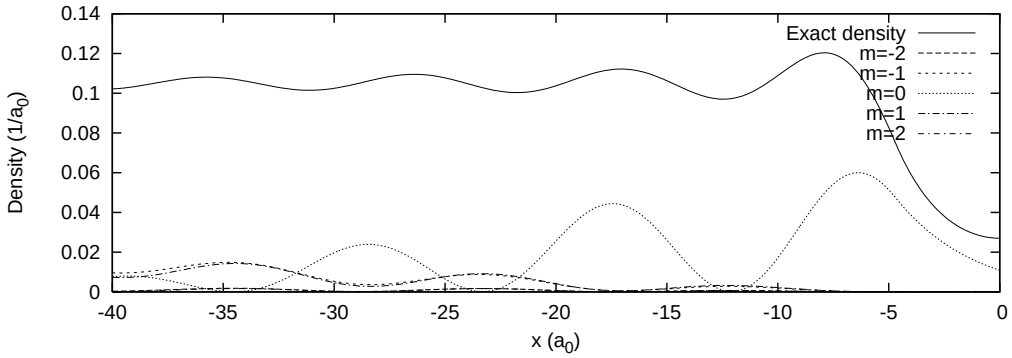

(a) Higher band

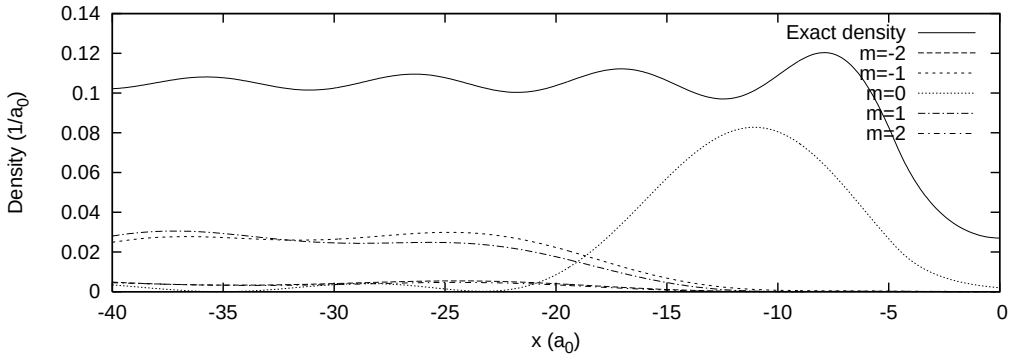

(b) Lower band

Figure 4.3: Individual wavepacket contributions to the total density for the two bands. Only the first few right-incident wavepackets are shown.

the transmitted side the density is built up mainly from the identical left-incident wavepackets (since there is little transmission through the barrier).

For both bands, the initial wavepacket is the major contributor close to $x = 0$. The two wavepackets propagated by one time step ($m = \pm 1$) are significantly more dispersed than the initial wavepacket and very similar in shape to one another; however, $m = 1$ has a smaller contribution due to a trasmitted component on the other side of the barrier. In the lower band these wavepackets are almost entirely contained within the plotted range, while in the higher band only the tails are visible. This is because the group velocity of the wavepackets is greater for higher energy bands[2]. The lower energy wavepackets also disperse more, since they include components which

[2]The group velocity for the higher band is $\sim k_{\mathrm{F}}$ and so the distance between wavepacket peaks is $\sim k_{\mathrm{F}}\tau_1 = 68a_0$. Instead, for the lower band the group velocity is $\sim k_{\mathrm{F}}/2$ and the distance between peaks is $\sim 34a_0$.

are almost stationary (for energies approaching zero).

The wavepackets propagated by two time steps ($m = \pm 2$) only make up a small contribution to the total density in this range, due to their propagation away from the barrier. The contributions from subsequent wavepackets will be even smaller. Therefore, it is clear why only a small number of wavepackets is needed to recover the local ground state density.

4.3 Scattering calculations

In the case of a system characterised by a Hamiltonian not equal to the reference Hamiltonian it is not sufficient to sum the wavepacket contributions to obtain the ground state density, since these will no longer be made up of eigenstates of the system (such as the scattering states of a square barrier). However, it is also possible to recover the density by scattering PWPs or SWPs through the system (provided of course that the potential is localised and becomes flat outside a central region). This can be understood by first considering the effect of occupying a single PWP with an electron and propagating this through a flat potential: the electron will move from one wavepacket to the next in time τ. Similarly, occupying a number of neighbouring wavepackets will result in each electron moving by exactly one wavepacket during each time step. Therefore, we can build up a current by placing a new electron at regular time intervals in the same wavepacket. This will eventually span the system, and the resulting electron density will be equal to the ground state density.

However, if the potential is not flat, the electrons will be scattered once they reach the barrier. The scattering process will result in the electrons being in a superposition of several PWPs, equal to a single SWP for that potential. After time τ, each electron will be in a different superposition, equivalent to the next SWP. Once an electron leaves the central region the superposition of PWPs in which it finds itself will stay constant, and simply shift through the basis functions as before. This means that propagating electrons through a system using the PWP basis is equivalent to occupying the SWPs constructed using the scattering potential. To demonstrate this, we consider the sodium atomic chain model used previously.

The energy spectrum up to E_{F} is divided into two bands (equivalent to the two used for the SWP calculation). However, it is now necessary to include higher energy bands, to allow for the scattering process. Four bands of width $\Delta\varepsilon = 0.02$Ha above E_{F} were included (covering the interval $[0.056, 0.136]$); higher energy bands were neglected. The electrons were placed in the $m = -10$ wavepacket in both bands. Fig. 4.4 shows the result of the scattering

simulation; the ground state density is correctly reproduced, although it is not as well converged as the density obtained by using an equivalent number of SWPs. This is to be expected, since the numerical propagation adds a further approximation to the results. The figure also shows the contribution to the total density from the two bands. The two main sources of error can thus be identified. The lower band contribution is accurate close to the barrier but rapidly divergent moving outwards. This is due to the high dispersion of the lowest energy wavepackets; therefore, a large number of them are needed to converge the result. Instead, the higher band contribution is very close to the exact one throughout the whole range but does not accurately reproduce oscillation peaks. This is due to the truncation of the basis set; in fact, since this band is close to E_{F} it requires a greater energy range to scatter precisely.

Plotting the band contributions against time (Fig. 4.5) is a useful way of

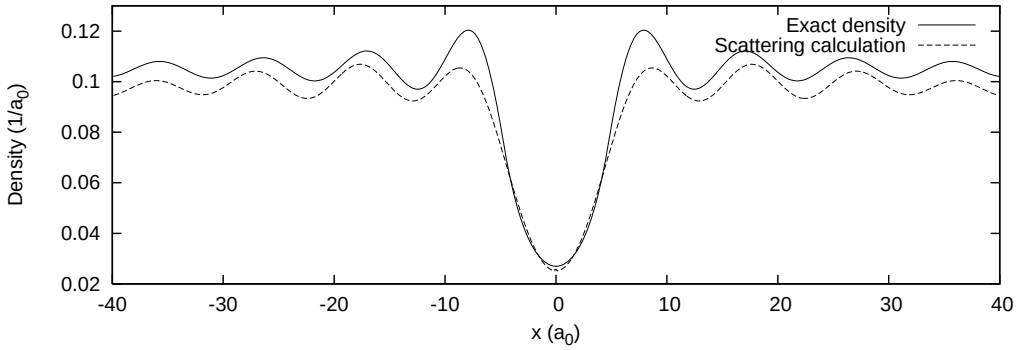

(a) Total density

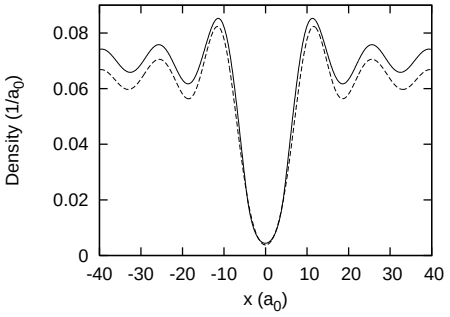

(b) Lower band contribution

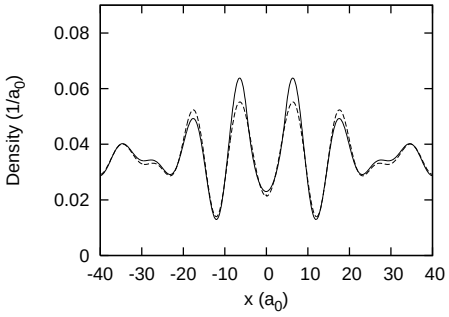

(c) Higher band contribution

Figure 4.4: Calculation of the ground state density using scattered PWP basis functions. In each graph the dotted line shows the PWP calculation and the solid line shows the exact result.

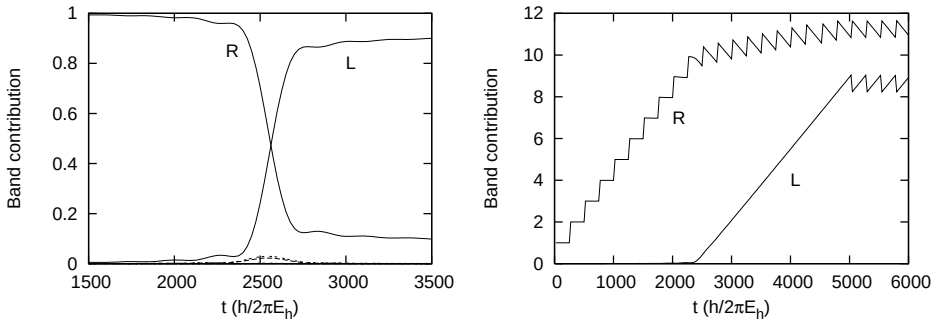

(a) Single electron (b) Electron current

Figure 4.5: Right and left-propagating energy band contributions changing with time in a scattering simulation.

visualising the propagation. The band contribution is calculated by summing the square of the coefficients of the state vector within each energy band. Right and left-propagating bands (with $\alpha = \pm 1$) are plotted separately. For the case of a single electron, the picture is simple: the right-propagating band in which it is originally placed is the only contributor until the electron approaches the barrier, at which point some of the total contribution passes to the equivalent left-propagating band (these contributions are similar to the reflection and transmission coefficients). Higher energy bands can be seen to have small contributions during the scattering process.

For the case of electrons being injected into the system, the total contribution is no longer constant; instead, it jumps by one every time a new electron is introduced. Therefore, the right-propagating band increases in steps until the first electron reaches the barrier. After this point the steps become distorted as the contribution from the left-propagating band increases. Finally, a steady state is reached after the first electron reaches the other end of the system and is removed.

4.4 Non-equilibrium simulations

4.4.1 Establishment of a steady current

The setup for many-electron simulations is discussed in Chapter 3. Unfortunately, due to the large computational cost of such simulations, only a limited number of energy bands and basis functions were used. Fig. 4.6 shows the initial electron density from a simulation using three bands: a full band, covering an energy range immediately below $E_{\mathrm{F}} = 0.5$Ha; a current band, in

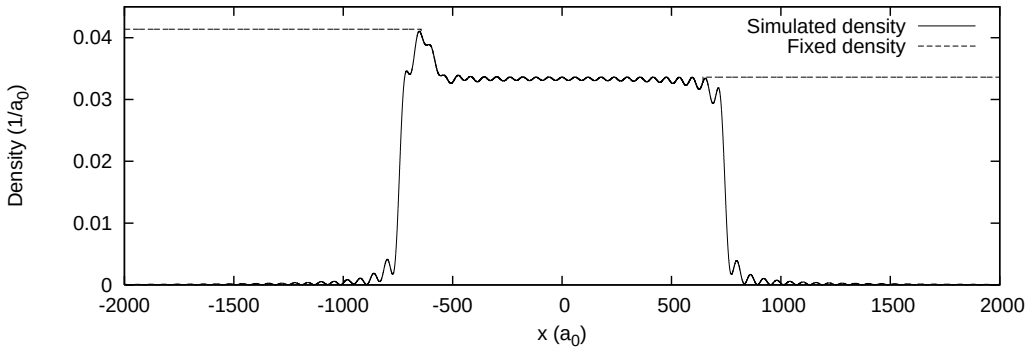

(a) $t = 0$

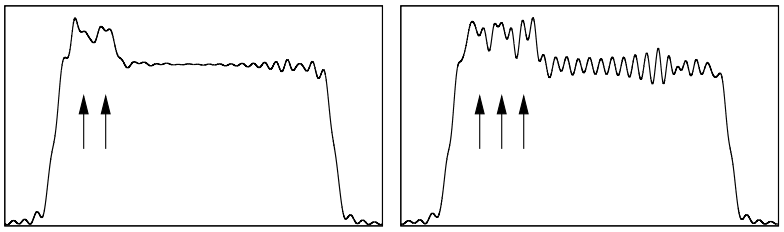

(b) $t = \tau$ and 2τ

Figure 4.6: Many-electron non-equilibrium simulation of the establishment of a steady current using a Hartree potential.

which electrons are injected into the system (covering a small energy range above E_{F}); and an empty band, covering a wide energy range above the current band to allow for scattering. As can be seen from the figure, the density in the buffer regions is fixed at different levels to account for the incoming current from the left. Once the first electron reaches the right buffer region, the levels become balanced. Since there is no external potential, the electron density is equal to the simplified Hartree potential. This is updated every 500 times steps ($\sim \tau/5$). The use of buffer zones is successful; in fact, the fixed density prevents the electrons from moving out of the real system.

The figure also shows the system after one and two time steps of the current band, illustrating the propagation of electrons to the right and introduction of new electrons from the left; two and three electrons can be seen respectively. However, during the simulation unphysical oscillations originate from the edges of the system; these can be seen to grow rapidly between time steps. Once the electron current spans the entire range of the simulation these artefacts prevent the observation of a flat density (as would be expected for a steady current). Fig 4.7 shows the evolution of the band contributions; this demonstrates that the simulation reaches a steady state, though not a

flat density.

These results suggest that a larger system is needed to observe the transient effects in the establishment of a current passing through an atomic point contact. However, the obtained results are nonetheless useful for studying the propagation of an electron front. In fact, with the addition of the Hartree potential the first electron in the current receives an acceleration from the one behind it, and therefore moves forward faster than its non-interacting counterpart.

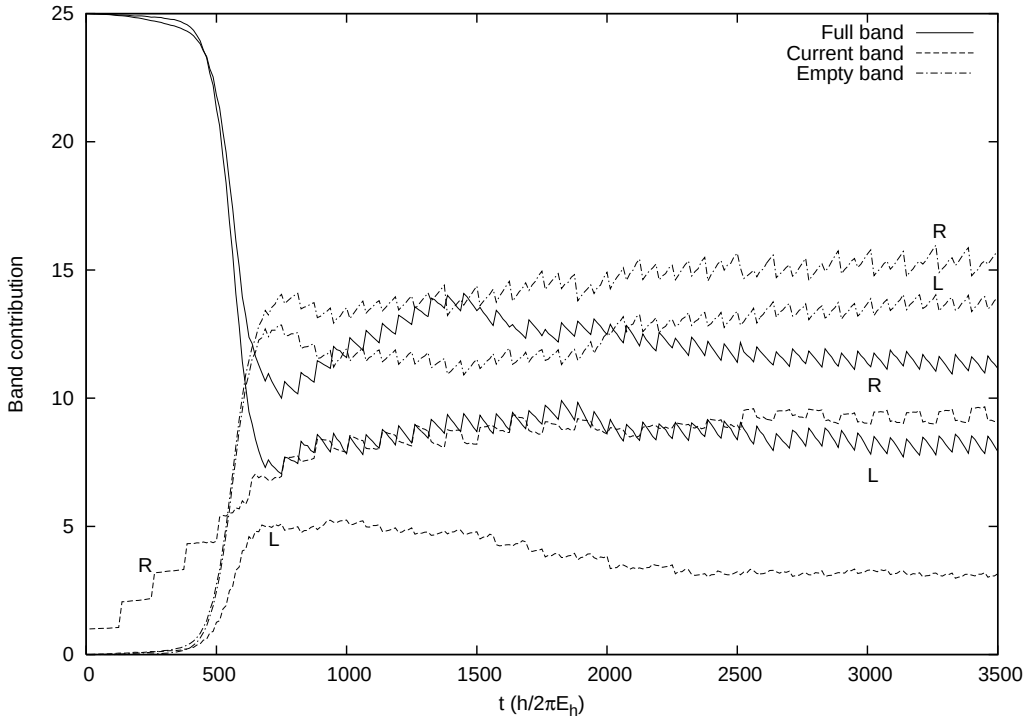

Figure 4.7: Energy band contributions changing with time during the establishment of a steady current. Electrons are added to the right-propagating current band. As can be seen, the propagation results in the electrons being in a superposition of wavepackets from all bands. Ideally, the lowest and highest energy bands should stay almost inert (i.e. completely full and completely empty respectively); the fact that this is not the case suggests that more bands need to be added to fully converge the results.

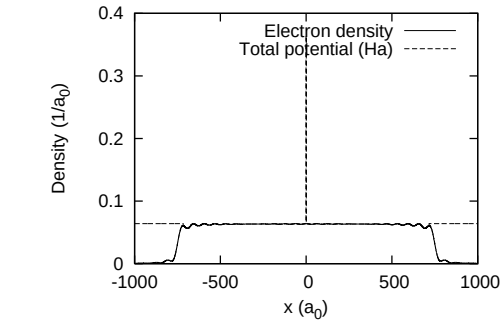

(a) Initial setup

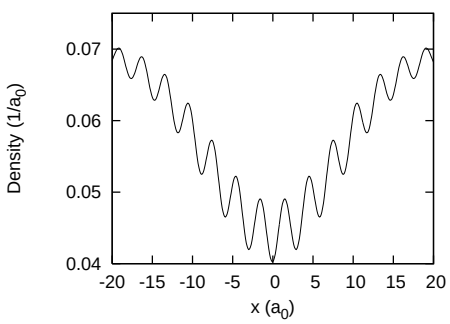

(b) Friedel oscillations

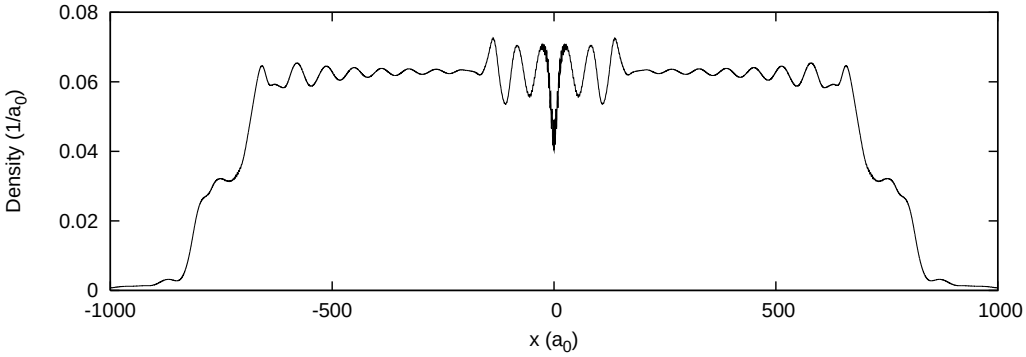

(c) Effect of the perturbing potential on the electron density after a short time

Figure 4.8: Many-electron simulation of the abrupt switching on of a potential barrier in a system in equilibrium.

4.4.2 Abrupt switching on of a potential

In this second type of simulation, the system initially has a flat potential and is in its ground state. For the example shown in Fig. 4.8, four PWP energy bands were used with the lowest two fully occupied ($E_{\mathrm{F}} = 0.6\mathrm{Ha}$). At the start of the simulation, a small and narrow potential barrier is introduced at the centre of the system (in this case, $V_0 = E_{\mathrm{F}}/2$). The resulting effect is a rapid oscillation spreading outwards from the barrier.

The figure shows how the system has evolved a short time after the introduction of the potential; the edge oscillations are still small and die away before reaching the real oscillations around the centre. However, the observed oscillations are not smooth; enlarging them reveals a second, higher frequency of oscillation that is being modulated. The wavelength of these faster oscillations is $\sim 2.8a_0$. As should be expected, this is approximately equal to the wavelength of Friedel oscillations in a Luttinger liquid (a model of interacting electrons in a 1D conductor, as is the case here) [23]. Friedel oscillations are

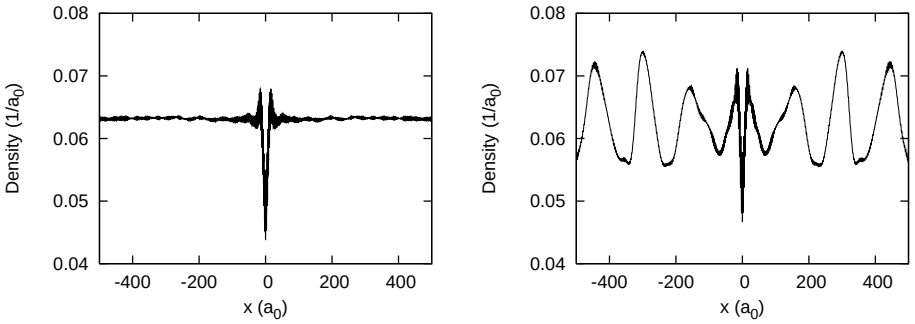

(a) Non-interacting (b) Interacting

Figure 4.9: Comparison of the ground state density obtained for a square barrier using interacting and non-interacting electrons.

observed around impurities (effectively point perturbations) with wavevector $2k_{\mathrm{F}}$. Therefore, for our system their wavelength is $\lambda = 2\pi/2k_{\mathrm{F}} = 2.89a_0$.

It is also important to consider the how the ground state density of a system changes between non-interacting and interacting electrons. Fig. 4.9 shows the steady state observed in a perturbing potential simulation for both cases; this is equivalent to calculating the ground state with a scattering method, since the central electrons will move out of the scattering region in a finite time[3]. It should be noted that for the interacting case the Hartree potential was modified respect to the previously discussed simulations. In order to eliminate the fast oscillations in the density from appearing in the potential a smoothing factor was introduced; this averages the density over a small range. In the case of a proper 2D or 3D Hartree potential, a similar smoothing effect is obtained automatically by the integration.

The figure shows large oscillations appearing in the interacting case that are absent in the non-interacting case. However, these oscillations are not static; instead, they propagate outwards continuously. Unfortunately, due to the small size of the system it is possible that the oscillations are unphysical and caused by edge effects. Further work is needed to properly converge these results.

4.4.3 Self-interaction

Finally, we consider the effect of spurious self-interaction on the propagation of wavepackets caused by the Hartree potential. Due to their highly localised

[3]This is the the same result proven by Stefanucci and Almbladh in the memory-loss theorem [24]. The theorem shows that the steady state of a system is independent of the history of the external perturbation.

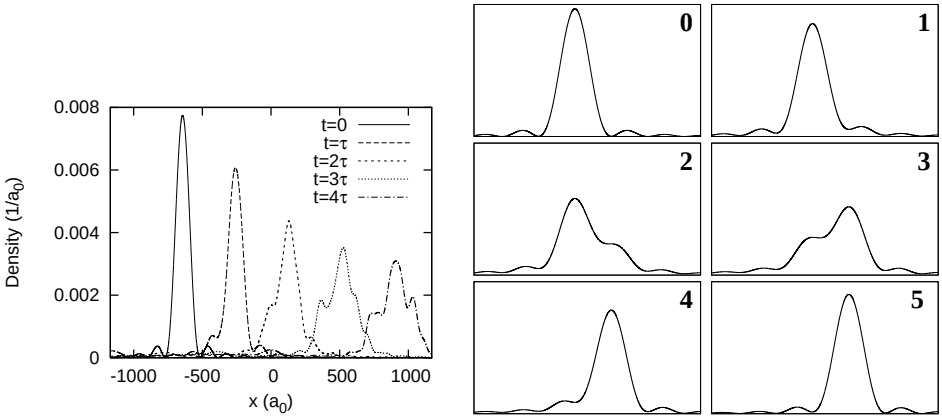

(a) Dispersion over 4 time steps (b) Evolution over a single time step

Figure 4.10: Effect of self-interaction on a single propagating electron.

nature, we expect this effect to be large. Fig. 4.10 shows the propagation of a single PWP in the energy band [0.5,0.55]. Since there is only one electron in the system, the true Hartree potential should be zero. The electron should therefore propagate exactly between wavepackets in time τ. Furthermore, over the short range plotted there is negligible dispersion between basis functions. Instead, the figure shows an extremely rapid dispersion, causing the initial wavepacket's amplitude to decrease by a factor of a half in about three time steps. The decrease in amplitude between time steps is greater for taller and narrower (i.e. more localised) wavepackets as expected. The figure also shows the motion of the wavepacket between time steps; instead of a constant and gradual dispersion (similar to the natural dispersion of the basis functions), the self-interacting wavepacket oscillates up and down with periodicity τ while propagating.

Another important effect of self-interaction is the unphysical acceleration received by the electron from its own repulsion. In fact, in our example the average speed of the wavepacket is $\sim 388 a_0/\tau$, three times greater than the speed of propagation without self-interaction ($\sim 129 a_0/\tau$).

Chapter 5

Conclusions

The results presented in the previous chapter illustrate the use of the novel stroboscopic wavepacket basis for the purpose of time-dependent calculations. In particular, it was shown that only a small number of basis functions are needed to calculate the non-interacting ground state density due to a localised potential, and that the correct density can be achieved by propagating wavepackets through the scattering region. The use of the basis for many-electron transport calculations was then demonstrated for the case of a 1D system coupled to bulk reservoirs of electrons.

The computational advantage of the basis set is also a conceptual advantage; in fact, the wavepacket description of non-equilibrium problems allows for a clear qualitative picture of the processes involved. This is due to the localised nature of the wavepackets, and, crucially, the stroboscopic construction of the basis. This property ensures that an electron in a wavepacket or a superposition of wavepackets will tend to stay in the same superposition, simply shifted within the basis set in discrete time steps. The superposition will only change when the electron encounters a difference between the potential of the system and the reference potential of the basis. In this respect, although PWPs are more useful for the physical understanding of the time evolution of the system, SWPs can be used to achieve a further significant reduction of the number of basis functions needed for an accurate simulation by choosing a reference potential as similar as possible to the system potential.

5.1 Accuracy and validity of results

As is always the case in computational experiments, the calculations need to be properly converged to obtain reliable results. In the case of ground state

density calculations (and in general any non-interacting scattering problem) this is achievable with a relatively small computational cost. This is not only due to the suitability of the basis set for such calculations but also to the fact that there are only two significant parameters: the range covered by the energy bands and the total number of basis functions. Although it is possible to choose the most convenient division of the energy range, in general using a smaller number of wide bands to cover the same range will result in a larger number of wavepackets needed in each band. For the special case of the reference potential being equal to the system potential this is reduced to a single parameter, since the energy range only needs to extend to E_{F}.

However, the computational cost significantly increases when considering interacting many-electron calculations. In particular, the discontinuity between the simulated scattering region and the bulk reservoirs in which electrons are assumed to propagate analytically causes unphysical oscillations to appear. In order to sufficiently reduce their amplitude the scattering region needs to be extended to reduce the discontinuity; of course, such an extension requires a greater number of basis functions. Further work in this respect is needed.

Apart from these computational considerations there are also a number of physical approximations that have not been addressed. Most importantly, the exclusion principle has not been implemented in the simulations. However, this can be corrected by extending the Hartree method to a full Hartree-Fock method with the use of Slater determinants. On the other hand, this would pose a practical problem when injecting electrons into the system, since only completely unoccupied wavepackets could be used. Another tacit assumption is the time-independence of the electron density in the analytic regions; this is necessary to exploit the properties of the basis set. In practice, it is a reasonable approximation provided that the reservoirs are broad compared to the scattering region.

5.2 Future work

The use of the stroboscopic wavepacket basis for quantum transport problems can be extended in several respects. Firstly, the construction of wavepackets starting from Bloch states instead of plane waves should be considered. Bloch states provide the eigenstates for a periodic potential system. Therefore, the analytic reservoirs on either side of the scattering region need not be restricted to having a flat potential; instead, a more realistic periodic potential could be employed. This would provide an additional similarity between the stroboscopic wavepackets and Wannier functions (however, contrary to

Wannier functions, the wavepackets are only approximately translationally invariant over short distances due to dispersion).

Furthermore, our time-dependent simulations can be applied to more complicated systems, such as 2D electron gasses and problems involving spin. Such simulations require a number of extra degeneracies to be included other than the direction of propagation of the wavepackets. In all these cases, including simple 1D systems, further work is needed to study the effects of localised negative potentials (or in general any potential supporting bound states); the propagation of electrons in such potentials is currently not well described by PWPs or SWPs alone.

Finally, considering the computational aspect of many-electron simulations, it should be noted that the methods used in our investigation are eminently parallelisable. In fact, the majority of the computational cost comes from the initial plotting of the basis functions and the recalculation of the potential matrix elements each time the Hartree potential is updated. Both tasks are made up of a large number of completely independent elements; these can easily be run on parallel nodes, with no intercommunication necessary.

Bibliography

[1] S. Datta and M. J. McLennan, Rep. Prog. Phys. **53**, 1003-1048 (1990).

[2] D. Goldhaber-Gordon, *Kondo Effect in a Single Electron Transistor* (Meeting Abstract, American Physical Society, 1998). Available from: `http://adsabs.harvard.edu/abs/1998APS..MAR..E302G`

[3] M. A. Kastner, Rev. Mod. Phys. **64**, 849 (1992).

[4] S. J. Tans *et al.*, Nature **386**, 474 (1997).

[5] S. A. Wolf *et al.*, Science **294** (5546), 1488 (2001).

[6] A. Bertoni *et al.*, Phys. Rev. Lett. **84**, 5912 (2000).

[7] B. J. van Wees *et al.*, Phys. Rev. Lett. **60**, 848 (1988).

[8] S. Datta, *Electronic Transport in Mesoscopic Systems* (Cambridge University Press, Cambridge, 1997).

[9] H. Mera, *Many-Electron Quantum Transport: Models and Theories* (PhD Thesis, The University of York, 2005).

[10] P. Hohenberg and W. Kohn, Phys. Rev. **136**, B864 (1964).

[11] W. Kohn and L. J. Sham, Phys. Rev. **140**, A1133 (1965).

[12] E. Runge and E. K. U. Gross, Phys. Rev. Lett. **52**, 997 (1984).

[13] N. Sai *et al.*, Phys. Rev. Lett. **94**, 186810 (2005).

[14] J. Werschnik, E. K. U. Gross and K. Burke, J. Chem. Phys. **123**, 62206 (2005).

[15] K. W. H. Stevens, J. Phys. C: Solid State Phys. **16**, 3649 (1983).

[16] G. H. Wannier, Phys. Rev. **52**, 191 (1937).

[17] A. Calzolari *et al.*, Phys. Rev. B **69**, 035108 (2004).

[18] A. A. Mostofi *et al.*, Comp. Phys. Comm. **178** (9), 685 (2008).

[19] T. Martin and R. Landauer, Phys. Rev. B **45**, 1742 (1992).

[20] P. Bokes, F. Corsetti and R. W. Godby, *Stroboscopic wavepacket description of non-equilibrium many-electron problems* (arXiv.org, `arXiv:0803.2448v1`, 2008).

[21] W. H. Press *et al.*, *Numerical recipes in C: The art of scientific computing* (Cambridge University Press, Cambridge, 1992).

[22] A. Castro, M. A. L. Marques and A. Rubio, J. Chem. Phys. **121**, 3425 (2004).

[23] R. Egger and H. Grabert, Phys. Rev. Lett. **75**, 3505 (1995).

[24] G. Stefanucci and C. O. Almbladh, Phys. Rev. B **69**, 195318 (2004).